DOI: 10.6060/mhc256432l

Paper/Статья

Porphyrins/Порфирины

Cu^{II} Porphyrin-Mediated Reed-Straw-Carbon-Based Cu-N-C Catalysts for Efficient Electrocatalytic Nitrate Reductions

M. Liu *et al.*

Cu^{II} Porphyrin-Mediated Reed-Straw-Carbon-Based Cu-N-C Catalysts for Efficient Electrocatalytic Nitrate Reductions

Mengyu Liu, Xinxing Shi, Xifeng Zhang, Jianming Lu, Weihua Zhu, and Xu Liang[@*]

School of Chemistry and Chemical Engineering, Jiangsu University, Zhenjiang 212013, China
[@]Corresponding to: E-mail: liangxu@ujs.edu.cn

Herein, the Cu^{II}porphyrin-mediated reed-straw-carbon-based Cu-N-C catalysts were prepared through high-temperature thermal treatment, and the structures were characterized bySEM, XRD, Raman, FT-IR and XPS. During the electrocatalytic experiments, Cu-N-C exhibits excellent nitrate reduction performance (56.33%) and high energy utilization efficiency (63.16%) at E = -1.3V. Also, the electrocatalytic stability and ion influence were also investigated. These results provide an opportunity to further explore the efficient electrochemical removal of nitride from M-N-C catalysts.

Keywords: Cu-N-C catalyst, nitrate reduction, electrocatalysis, biomass carbon.

Катализаторы Cu-N-C на основе Cu^{II}-порфирина и углерода из тростниковой соломы для эффективного электрокаталитического восстановления нитратов

М. Лиу, С. Си, С. Жанг, Дж. Лу, В. Жу, С. Лианг@*

При высокотемпературной термической обработке получены катализаторы Cu-N-C на основе порфирината Cu^{II} и углерода из тростниковой соломы. Их структуры были охарактеризованы с помощью сканирующей электронной микроскопии, рентгеновской дифракции, инфракрасной спектроскопии с преобразованием Фурье, рентгеновской фотоэлектронной спектрометрии. Cu-N-C демонстрирует превосходную производительность электрокаталитического восстановления нитрата (56,33%) и высокую эффективность использования энергии (63,16%) при E = -1,3 В. Также были исследованы электрокаталитическая стабильность и влияние ионов. Эти результаты открывают возможность для дальнейшего изучения эффективного электрохимического удаления нитрида из катализаторов M-N-C.

Ключевые слова: Катализатор Cu-N-C, восстановление нитрата, электрокатализ, углерод биомассы.

Introduction

Nitrate (NO_3^-) is the core carrier of nitrogen cycling in nature and has a profound impact on ecological balance and human activities. In agriculture, it serves as a key nitrogen fertilizer component, supporting global food production; in industry, it is used to manufacture fertilizers, explosives, and chemicals, driving economic development.[1-3] Unfortunately, the excessive entry into water bodies (such as rivers and lakes) can firstly promote the overgrowth of aquatic organisms such as algae.[4] Secondly, the excessive use of nitrogen fertilizer or sewage discharge in agriculture can lead to nitrate infiltration into groundwater, making long-term pollution difficult to purify naturally and affecting ecological balance.[5] Thirdly, excessive nitrate has public health risks, such as causing blue baby syndrome in infants, and long-term intake increases the risk of gastric and esophageal cancer.[6] Therefore, the World Health Organization (WHO) stipulates that the concentration of nitrate in drinking water should be below 50 mg/L (calculated as NO_3^-), and any excess should be treated.[7] In addition, there are clear regulations regarding nitrate in industrial and agricultural production activities. For example, industrial wastewater (such as electroplating, explosive manufacturing, chemical production) contains high concentrations of nitrate and requires pre-treatment before discharge.[8-10] Especially in industries such as semiconductor manufacturing and pharmaceuticals, which have extremely high-quality water requirements, nitrate as an impurity may affect product quality.[10-11] Also, the overcome accumulation of nitrate in agricultural production management can lead to soil acidification, damage soil structure, and affect crop growth. Reducing nitrate leaching can improve nitrogen fertilizer utilization efficiency, lower costs, and reduce environmental pollution.[12-15]

In order to highly efficient removal of nitrate, a series of methods have been demonstrated in the past, for example: researchers have been using biological denitrification, and nitrate is converted into nitrogen (N_2) by microorganisms and released into the atmosphere.[16-17] Also, adsorption of nitrate ions through resin is suitable for small-scale water treatment,

but utilizing reverse osmosis/electrodialysis membrane separation technology is efficient but costly.[18-19] At the same time, we use chemical reduction to convert nitrate ions into harmless substances using reducing agents such as iron and hydrogen.[20] Recently, M-N-C catalysts are the hybrid material composed of transition metals (M, such as Fe, Co, Ni, Mn, Cu, *etc*.), nitrogen (N), and carbon (C)[20-21] that have received widespread attention in the fields of energy conversion and storage (such as fuel cells, metal air batteries, electrolyzed water, *etc*.) due to excellent electrocatalytic performance (such as oxygen reduction reaction, ORR), high stability, and low cost.[22-24] For example: M-N-C catalysts (such as Fe-N-C) are an ideal choice to replace precious metal platinum (Pt) catalysts in fuel cells and metal air batteries, significantly reducing costs;[25] some M-N-C materials, such as Ni-N-C and Co-N-C, can efficiently convert CO_2 into fuels such as CO and CH_4;[27-28] some M-N-C materials (such as Co-N-C) exhibit bifunctional catalytic activity in hydrogen evolution reaction (HER) and oxygen evolution reaction (OER).[29-30] In addition, M-N-C catalysts can also be applied to nitrogen reduction reactions (NRR), organic molecule oxidation, and other applications.[30] On the hand, M-N-C catalysts are also widely applied in the electrochemically catalyzed nitrite reductions, and their tunable and enhanced catalytic performance could be modulated by transition metal center, the synergetic effect of dual-metal centers, the coordination number of nitrogen atom and doping elements (such as S, P).[31-33] More importantly, the hierarchical pore structure (microporous/mesoporous) and high specific surface area carbon substrate (such as ZIF-8 derived carbon) of M-N-C materials based on porous carbon skeleton design can provide more $M\text{-}N_x$ site anchoring points, increase active site exposure, promote reactant diffusion and product desorption.[34-38] Herein, we use naturally abundant reed-straw to prepared porous carbon substrate, and the Cu(II) porphyrin mediated reed-straw-carbon-based M-N-C catalysts were prepared through high-temperature annealing treatments. Also, their electrochemically catalyzed nitride reductions were also evaluated.

Experimental

Material and Instruments

A UV-Vis spectrophotometer (TU-1810, Persee) was used to determine the concentrations of nitrate, nitrite and ammonium (Text S1, Figure S1, S2, S3, see *Supporting Information*). The catalyst was tested using a scanning electron microscope, energy dispersive spectrometer (SEM/EDS, JSM-6010PLUS/LA). X-ray photoelectron spectroscopy (XPS, Thermo-Escalab 250Xi) was used to determine the elements C, N, Cu and Ni in the catalysts. The catalysts were tested by X-ray diffraction (XRD, Shimadzu 6100), which is equipped with high intensity Cu-Kα radiation. Fourier transform infrared spectroscopy (FT-IR, Nicolet Nexus 470) was used to test the infrared spectra of the catalysts (KBr pressed slices). Raman measurements were made on a Thermo Scientific DXR Smart Raman spectrometer using a 532 nm laser (Raman, Thermo Scientific DXR). Electrocatalytic nitrate testing was carried out on an

electrochemical analyser (CHI-730D, CHI-604E) in a three-electrode system. Herein, the production of NO and NO_2 was negligible. In this paper, a NO_3^--N solution with a concentration of 100 mg/L was prepared with ultra-pure water and sodium nitrate, which was used as nitrate wastewater in the electrolysis experiment, with sodium chloride as electrolyte (0.1 mol/L). Nitrate reduction ($R_{NO_3^-}$), total nitrogen removal (R_{TN}, total nitrogen as nitrate, nitrite, ammonium), N_2 selectivity (S_{N_2}), reaction rate and energy utilization efficiency were calculated according to the following equations (Eq. 1-7):

$$R_{NO_3^-}(\%) = ((NO_3^-)_o - (NO_3^-)_f)/(NO_3^-)_f \quad (1)$$

$$R_{TN}(\%) = ((NO_3^-)_o - (NO_3^-)_f - (NO_2^-)_f - (NH_4^+)_f)/(NO_3^-)_o \quad (2)$$

$$S_{N_2}(\%) = (NO_3^-)_o - (NO_3^-)_f - (NO_2^-)_f - (NH_4^+)_f/(NO_3^-)_o \quad (3)$$

$$\eta = [(Q(NO_2^-)_f) + Q(N_2)_f + Q(NH_4^+)_f]/Q_f \quad (4)$$

$$Q(NO_2^- - N)_t = 2F(C(NO_2^-)_f V/M) \quad (5)$$

$$Q(NH_4^+ - N)_t = 8F(C(NH_4^+)_f V/M) \quad (6)$$

$$Q(N_2 - N)_t = 5F[(C(NO_3^-)_o - C(NO_3^-)_f - C(NO_2^-)_f - C(NH_4^+)_f)V/M] \quad (7)$$

Here, the subscripts 'o' and 'f' indicate the initial and final states, respectively. Details of energy utilization efficiencies and pseudo first-level kinetic can be found in the *Supporting information*.

Preparation of M-N-C catalysts and working electrodes

The reed straw (RS) was collected from the riverside of the Yangze River of Zhenjiang, China. As shown in Scheme 1, the RS was dried and crushed into powder, and an appropriate amount of the powdered reed straw was hydrothermally treated at 150 °C about 24 h by using a reactor equipped with a polytetrafluoroethylene liner. Then, the samples were taken out for washing, filtration, dry and pyrolysis at 800 °C in a tubular furnace to obtain a black powder sample of reed straw carbon (RSC). In addition, the Cu-N-C catalyst was obtained by mixing 20 mg Cu^{II} tetraphenylporphyrin (Cu^{II}TPP) with 100 mg RSC in 20 mL of CH_2Cl_2 and annealing at high temperature in a tube furnace after treatment (Scheme 1). The Carbon paper (0.5×0.5 cm) was used as the substrate for the electrodes. The carbon paper was sonicated with ethanol, acetone and ethanol for 10 min before use. Then, 1 mg of catalyst was mixed in 0.4 mL of isopropanol with 10 μL of nafion solution, applied dropwise to both sides of carbon paper and dried in an oven at 60 °C for 2 h to obtain a working electrode.

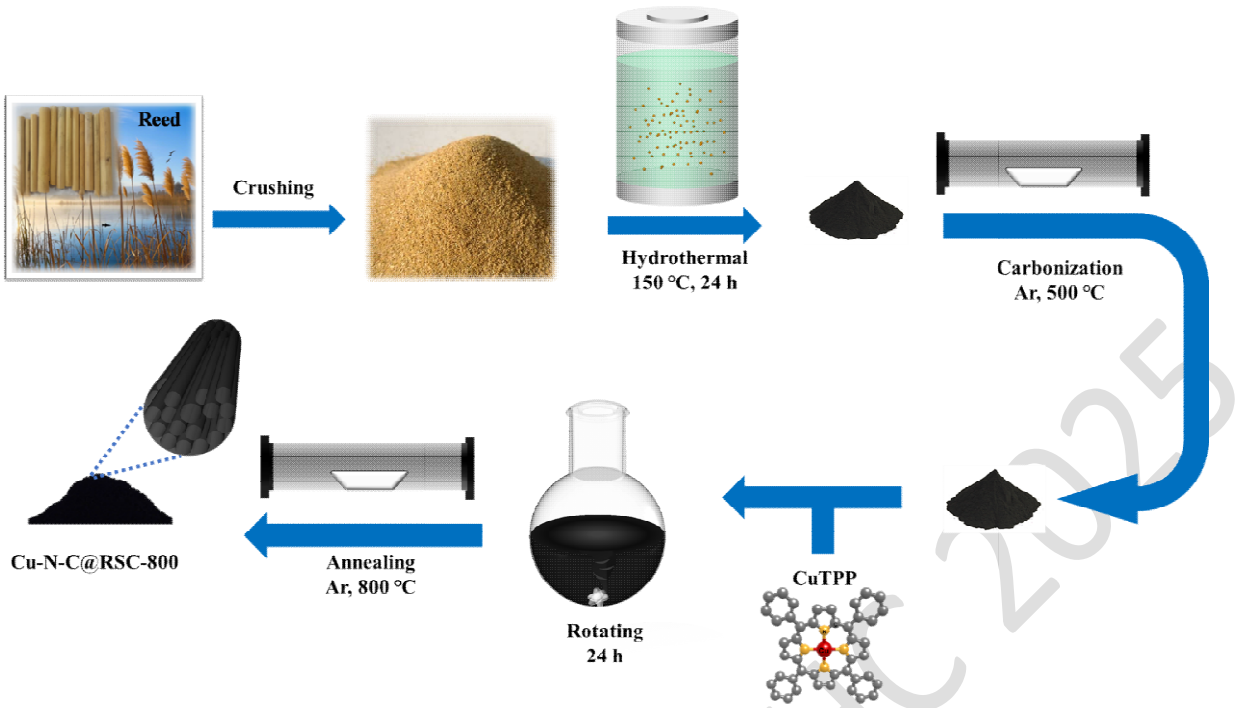

Scheme 1 Preparation of Cu^{II}porphyrin-mediated reed-straw-carbon-based Cu-N-C catalysts.

Results and Discussion

Structural Characterizations

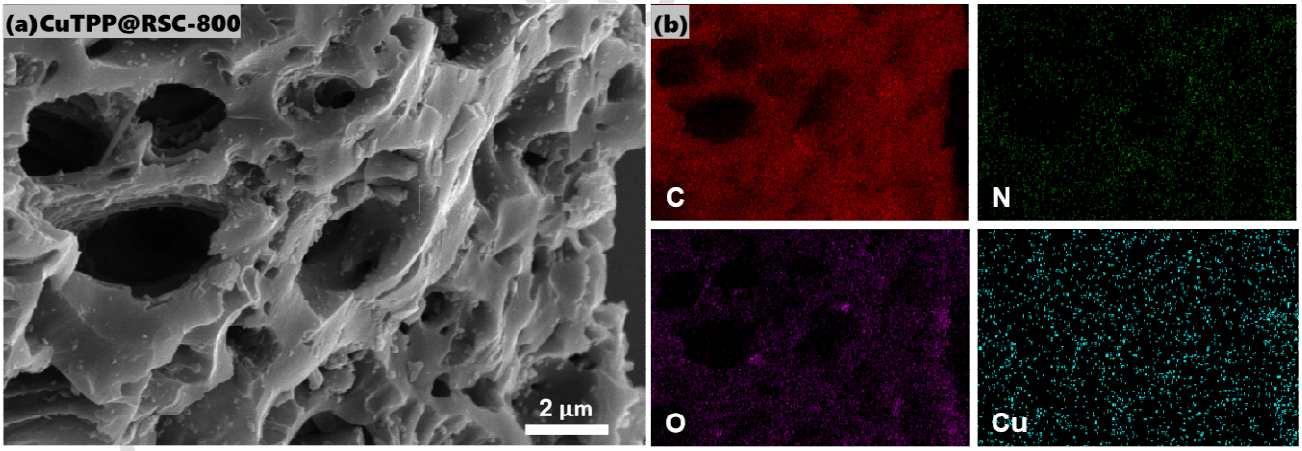

Figure 1 (a) SEM images and (b) elemental distributions of Cu-N-C@RSC-800.

Morphology Confirmation. Under scanning electron microscopy investigations, the reed straw carbon shows a well-defined pore structure with 2-5 μm diameters, which is originally from the natural structure of fresh reed straw (Figure 1a, corresponding reference see Figure S4). Importantly, the clear porous structure can prevent agglomeration and increase NO_3^- ionic adsorptions, which potentially enhances electrochemically catalyzed NO_3RR reactivity. Also, the well-performed pore structures are indicating the suitable thermal stability during the high-temperature annellation. On the

other hand, the elemental distributions of C, N, O and Cu in the Cu-N-C catalysts, the energy disperse spectroscopy (EDS) mapping analysis was investigated. First, the ratio of C in the RSC is 78.4%, and then it is increased to 89.25%. On the contrary, the ratio of O is decreased from 20.32% to 7.57%. Those all indicates the change of RSC elements constitution during annealing. In Figure 1b, the C, N, O and Cu elements are uniformly distributed in the reed straw carbon substrate, and no aggregation or agglomeration was observed.

In order to confirm the crystallographic structure of Cu-N-C@RSC Cu-N-C catalyst, we compare the X-ray diffraction (XRD) patterns of the RSC and the Cu-N-C@RSC Cu-N-C catalyst. As shown in Figure 2, these two samples have wider diffraction peaks at 2θ = 23º and 44º, which are belonging to the characteristic peaks of graphite carbon (002) and carbon (101) crystal surfaces. This result indicates the graphite properties and excellent conductivity of the Cu-N-C catalyst. Meanwhile, these two samples don't have any characteristic peaks of metal clusters that indicating no aggregation was observed. On the other hand, by comparing the FT-IR spectra of RSC, Cu-N-C catalyst, and Cu^{II}tetraphenylporphyrin (CuTPP) (Figure 2b), the porphyrin skeleton vibration peaks of CuTPP were appeared at around 1000 cm^{-1}, which disappeared in other samples indicates that the structure of CuTPP had been completely destroyed during high-temperature annealing. In addition,we consulted relative references. According to TGA results, we could find that the weight loss of CuTPP has reached 95% of its origin weight at 668 ℃, which can prove the structure of CuTPP has been broken during thermal annealing at 800 ℃ (Figure S5). Compared with RSC, it can be seen that the infrared characteristic peaks of Cu-N-C are basically consistent with those of the carrier, which also indicates that the main structure of the carbon substrate can still be maintained after annealing.

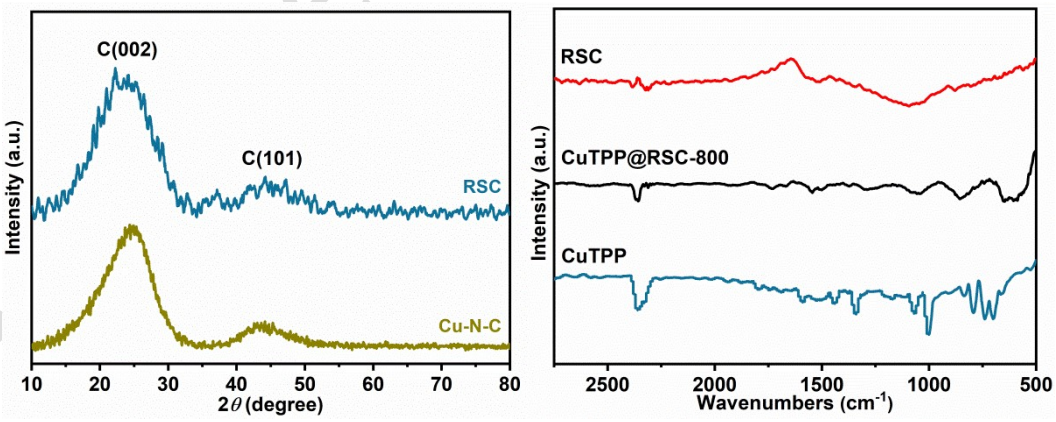

Figure 2. X-Ray diffraction (XRD) patterns of RSC (top) and Cu-N-C (bottom).

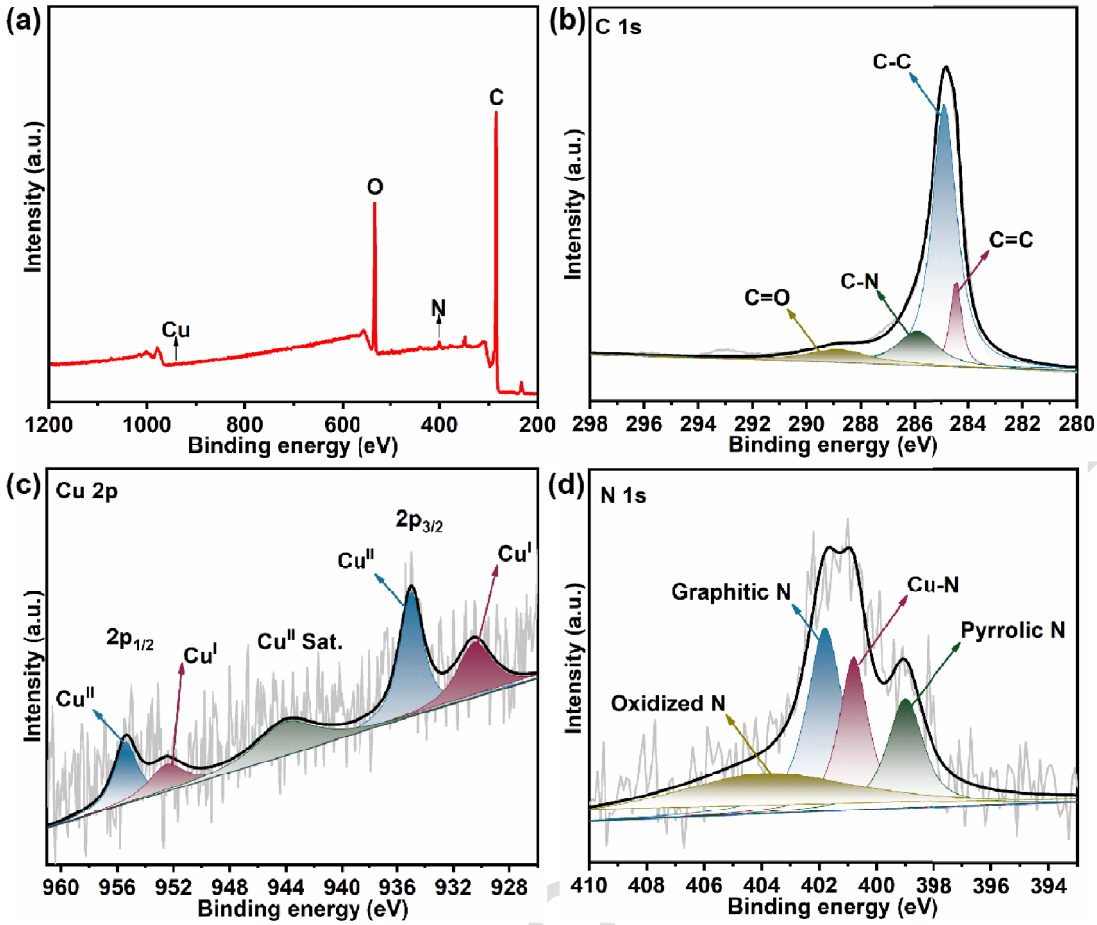

Figure 3. (a) – XPS analysis of Cu-N-C. (b-d) – XPS spectra of C1s, N 1s and Cu 2p.

To further understand the element distribution and existence state, the X-ray photoelectron spectroscopy (XPS) was tested. In Figure 3a, the full XPS spectra is composed of the characteristic peaks of C, O, N and Cu elements from the Cu-N-C catalyst, which were in good agreement with EDS mapping analysis. In addition, the assignment of C 1s, Cu 2p and N 1s orbitals were also investigated to confirm the formation of all elements. Firstly, the C 1s assignment (Figure 3b) of Cu-N-C catalyst has C-C (284.9 eV), C=C (284.4 eV), C-N (285.9 eV) and C=O (288.8 eV) peaks. Secondly, the Cu 2p assignment has a set of peaks corresponding to Cu element, which were attributed to the Cu^{2+} (935.0 eV) and Cu^{+} (930.4 eV) peaks from Cu $2p_{3/2}$ orbital, and the Cu^{2+} (955.4 eV) and Cu^{+} (952.3 eV) peaks from Cu $2p_{1/2}$ orbital. Notedly, it can be seen that both Cu^{2+} and Cu^{+} are presented in the catalyst, and the Cu^{2+} is the main component in the Cu-N-C catalyst. Also, the N 1s spectra has the signal peaks at 403.7 eV, 401.8 eV, 399.0 eV, and 400.8 eV that are assigned for oxidized nitrogen N, graphite N, pyrrole N, and Cu-N, respectively. It should be noted here, graphitic N is beneficial for accelerating electron transfer, while pyrrolic N is beneficial for promoting nitrate adsorption ability during electrocatalytic processes, and is consistent with the M-N coordination present in Cu-N-C catalysts.

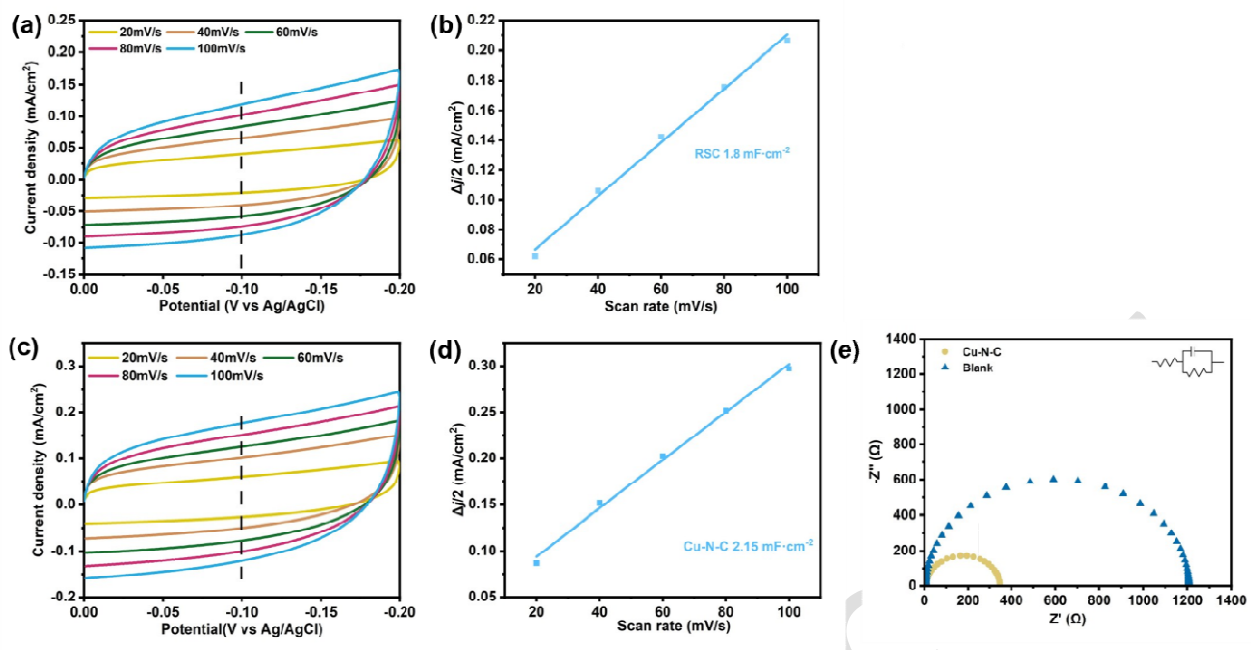

Figure 4. (a),(c) – Cyclic voltammograms of Cu-N-C and blank sample at various scan rates from 20 to 100 mV/s between 0 ~ -0.2 (V *vs*. Ag/AgCl). (b),(d) – Corresponding double-layer charging current against the scan rate. (e) – Electrochemical impedance spectra of the Cu-N-C and blank sample.

In addition, we measured the double-layer capacitance (Cdl) via cyclic voltammetry (CV) and utilized this parameter to calculate the electrochemically active surface area (ECSA) of Cu-N-C and RSC catalysts. As shown in Figure 4, Cdl values of Cu-N-C and RSC are 2.15 and 1.8 mF· cm^{-2}, respectively. According to ECSA = $\frac{Cdl}{Cs}$, we can see that Cu-N-C has a larger electrochemical active surface area. In fact, we can assume that the active sites both of them are roughly equal due to similar Cdl values, which indicates the origin structure of RSC determined the final morphological features of Cu-N-C including ECSA. Then, in an electrolyte solution with a nitrate concentration of 100mg/L and containing 0.1M Na_2SO_4, within the frequency range of 100 kHz to 0.1Hz, with a signal amplitude of 10 mV and a potential of -1.3V (*vs*. Ag/AgCl), the conductivity of Cu-N-C was investigated through electrochemical impedance testing. As the Nyquist diagram shows, a semicircle can be observed in the high frequency range, which represents the charge transfer process, and the diameter of the semicircle shows the charge transfer impedance (R_{ct}).The Nyquist diagram shows that Cu-N-C has the smallest charge transfer resistance (R_{ct}) than blank sample, indicating that it has good electrical conductivity, which is also the reason for the enhanced performance of NO_3^-RR.

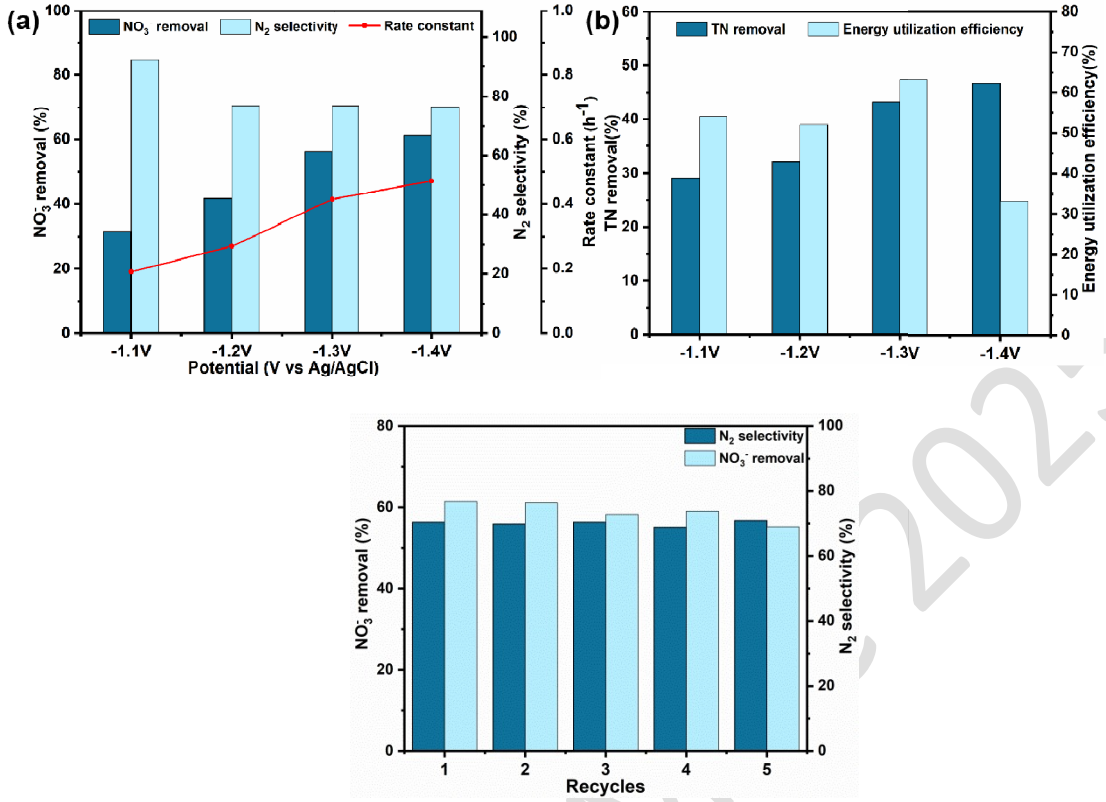

Figure 5 Effect of potential on (a) nitrate reduction, N_2 selectivity, and rate constant, and (b) TN removal and energy utilization efficiency (Initial nitrate concentration 100 mg/L); (c) Nitrate removal capacity and nitrogen selectivity over 5 cycles test of electrocatalytic denitrification (Initial nitrate concentration 100 mg/L, 4 h of operation for each cycle, E = -1.3 V vs Ag/AgCl).

During electrocatalytic process, the influence of voltage constant is greatly affected. Thus, the optimal constant voltage for removing nitrate ions was tested through a series of different constant voltages (E = -1.1, -1.2, -1.3, -1.4 V; *vs* Ag/AgCl). As shown in Figure 5a, upon increasing the controlled potentials from E = -1.1 to -1.4 V, the removal efficiency of NO_3^- ions increased from 31.5% to 61.1%, and the N_2 selectivity are all overcome 70%. Thus, it has been demonstrated that the electrocatalytic nitrate reductions followed a pseudo first order kinetic model, with corresponding reaction rate constants ranging from 0.19 h^{-1} (E = -1.1 V) to 0.41 h^{-1} (E = -1.3 V). Notably, a significant increase of rate constant was E = -1.2 to -1.3 V, but the mirror changes were appeared between E = -1.3 to -1.4 V probably due to the competitive water-splitting reactions are becoming more favorable.

Meanwhile, the removal efficiency of total nitrogen (TN, Figure 5b) was also increased from 29.1% (E = -1.1 V) to 46.7% (E = -1.4 V). The energy utilization efficiency was estimated based on the changes in inorganic nitrogen during the electrochemical reduction process, and highest utilization efficiency 63.2% was obtained when the controlled potential was arranged at E = -1.3 V. Based on the above nitrate reduction performance and energy utilization efficiency, E= - 1.3 V is a

more reasonable voltage and is used for subsequent electrochemical reactions. As shown in Figure 5c, long-time stability test is also an important method to evaluate the nitrate removal ability and catalyst performance. Under the conditions of an initial nitrate concentration of 100 mg/L and a constant voltage of -1.3 V *vs* Ag/AgCl, the nitrogen selectivity remained at around 56% after 5 cycles, and the nitrate removal ability was also around 76%. This indicates that the catalyst not only has excellent nitrogen selectivity, but also demonstrates its good stability.

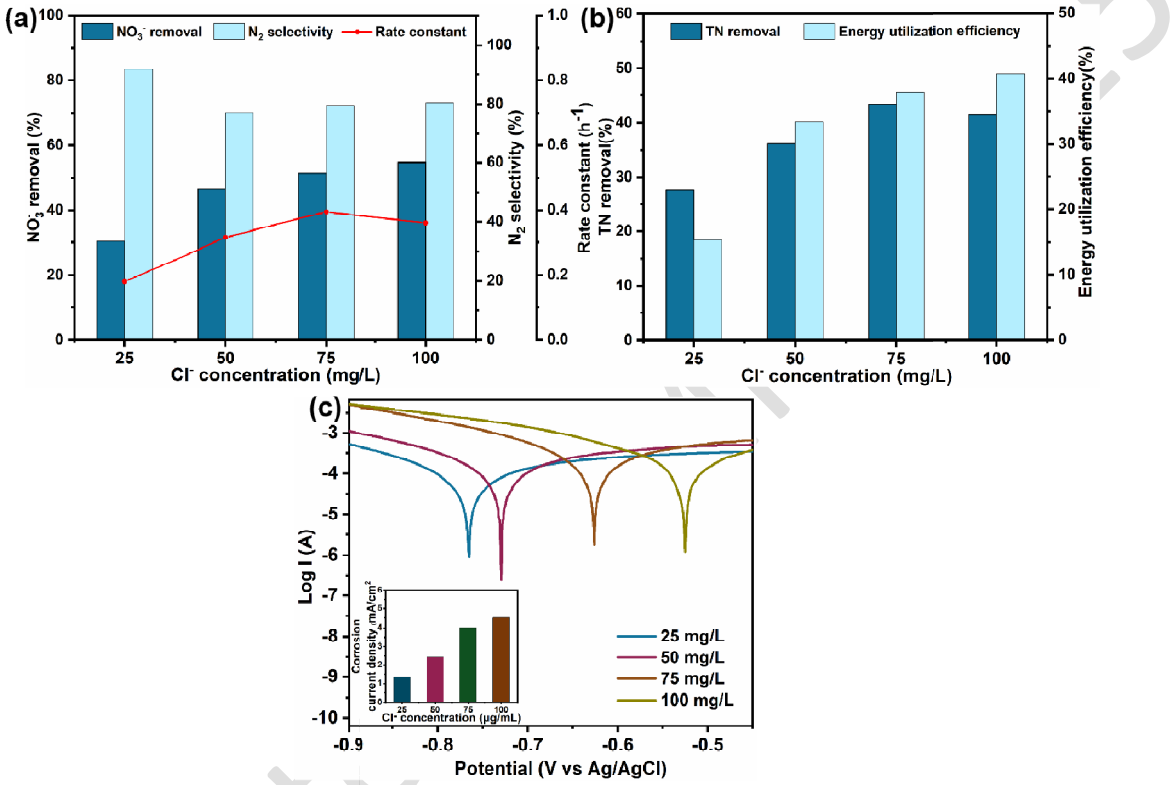

Figure 6. Effect of initial chloride concentration on (a) nitrate reduction, N_2 selectivity, and rate constant, and (b) TN removal and energy utilization efficiency. (c) – Potentiodynamic polarization curves of Cu-N-C at different chloride concentration (Initial nitrate concentration 100 mg/L).

The chloride ion will tend to be oxidized into chlorine gas which could react with H_2O to form hypochlorous acid. In fact, reactions mentioned above also happen during electroreduction process, and the formed hypochlorous acid is conducive to turning NH_3 into N_2. However, when the content of NaCl in the solution is too low, the amount of HClO generated will not be enough to oxidize all the generated ammonia nitrogen. Certainly, if too much NaCl added, generating too much ClO^- may oxidize nitrite to nitrate, while ClO^- and Cl^- compete with nitrate for adsorption, inhibiting nitrate removal.Therefore, it is necessary to investigate the effect of Cl^- concentration on the electrochemical reduction process of nitrate ions. On the basis of simulating nitrate wastewater, different concentrations of Cl^- were added, and the experimental

results are shown in Figure 6(a-b). When the Cl^- concentration is 25, 50, 75, and 100 mg/L, the removal rates of nitrate ions are 30.25%, 46.74%, 54.63%, and 51.35%, respectively, and the energy utilization rates are 15.27%, 33.43%, 37.97%, and 40.74%, respectively. The results showed that the electrochemical reduction of nitrate was most effective when the Cl^- concentration was 75 mg/L. Comparing the effects of initial chloride concentrations of 0 g/L and 0.1 g/L on nitrate reduction, it was found that the addition of Cl^- slightly reduced the ability to reduce nitrate. During the reaction process, Cl^- corroded the Cu-N-C catalyst, weakening its reducing ability. From Figure 6c, it can be seen that with the increase of Cl^- concentration, the corrosion current density increases and the removal rate of nitrate ions also decreases. Therefore, adding an appropriate amount of Cl^- during the electrocatalytic reduction process will reduce the ability to catalyze nitrate ions due to the corrosion of the electrode by Cl^-. However, according to the break point chlorination theory, Cl^- can make NH_4^+ more easily converted to nitrate ions during the catalytic process, resulting in an antagonistic effect of Cl^- addition on nitrate reduction. So, choosing the appropriate Cl^- concentration is extremely important. Based on the comprehensive consideration of nitrate removal and nitrogen selectivity, the optimal Cl^- ion concentration is 75 mg/L.

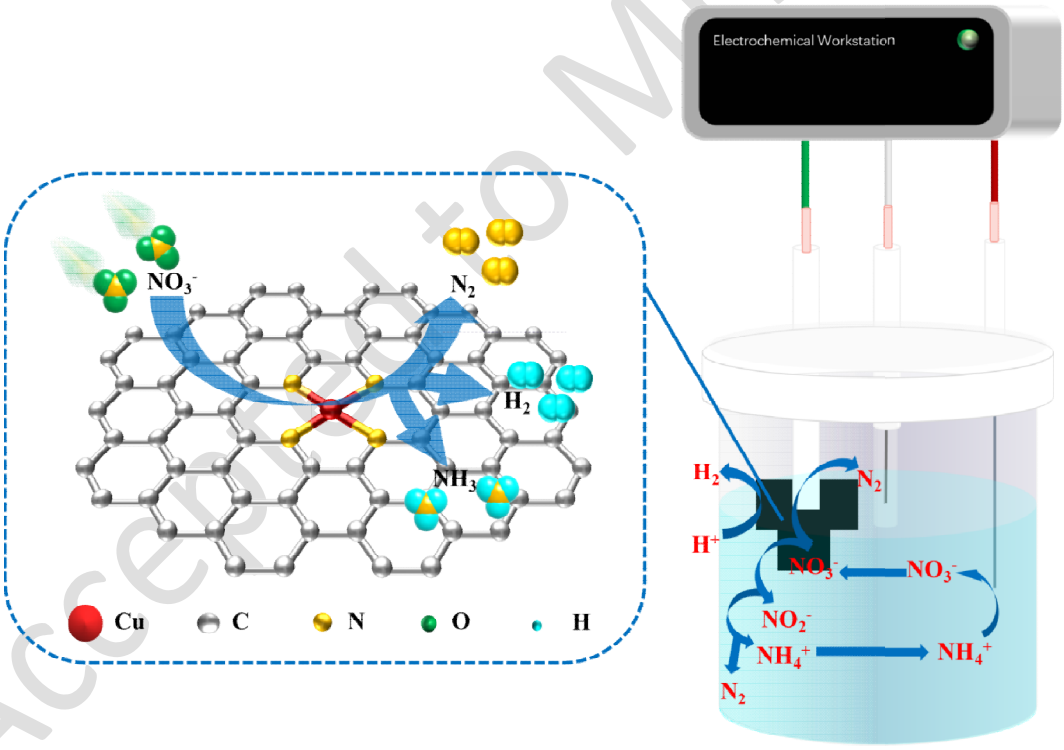

Scheme 2 A plausible mechanism of Cu^{II}porphyrin-mediated reed-straw-carbon-based Cu-N-C catalysts for electrocatalytic NO_3^- reductions.

Conclusion

In summary, this article utilizes the biomass resource reed straw with abundant yield and low utilization rate to prepare porous carbon as a loading substrate for metal copper porphyrin. After secondary annealing at 800 ℃, Cu-N-C

catalyst is prepared. Furthermore, we characterized the morphology and electronic structure of Cu-N-C catalyst using SEM, XRD, Raman, FT-IR, and XPS. In electrochemical measurements, Cu-N-C has a larger catalytic active area and smaller charge transfer resistance. Under electrochemical catalysis, Cu-N-C catalyst exhibits the best catalytic performance at E = -1.3 V (*vs* Ag/AgCl), with nitrate reduction ability and energy utilization rate of 56.33% and 63.16%, respectively. In addition, when the Cl^- concentration was 75 mg/L, the Cu-N-C catalyst exhibited the best catalytic performance in simulated nitrate wastewater and showed good chemical stability testing, proving that the catalyst remained stable not only during the catalytic process, but also in multiple cycles. Considering the outstanding performance of M-N-C catalyst in multiple fields, this study opens up new ideas for the application of electrocatalytic nitrate reduction and provides important references for the rational design of bio based Cu-N-C materials.

Acknowledgements. This work was supported financially by the NaturalScience Foundation of China (21701058), Jiangsu University (17JDG035), the Innovation Project of JiangsuProvince 2023 and the Educational Science Planning Project of Jiangsu Province (B/2022/01/129).

Conflicts of interest. The authors can declare that there are no known competing personal relationships or financial interests that could be perceived as having influenced the research reported in this study.

Author contributions. Mengyu Liu, Xinxing Shi, focused on the material preparation and electrochemical characterizations; Xifeng Zhang were Jianming Lu focused on the electrochemical characterizations; Weihua Zhu and Xu Liang focused on the manuscript preparation and the whole work was well discussed byall authors

References

1. Lim J., Fernández C.A., Lee S.W., *et al. ACS Energy Lett.* **2021**, *6*, 3676-3685.
2. Chuan D. Z., Yu C., Qian Y., et al. *J. Phys. Chem. C* **2019**, *123*, 27286-27294.
3. Hou P.F., Yuan W.S., Li G.H., et al. *Agron. J.* **2021**, *113*, 5027-5039.
4. Xin X., Yi Y.Z., Hong R P., et al. *Environ. Sci. Technol*. **2025**, *59*, 467-477.
5. Jun J.W., Xiao C.L., Beusen A.H.W., et al. *Environ. Sci. Technol*. **2023**, *57*, 19395-19406.
6. Kalaycıoğlu Z., Erim F.B. *J. Agric. Food Chem*. **2019**, *67*, 7205-7222.
7. *Guidelines for drinking-water quality*: 4th edition incorporating the 1st and 2nd addenda, https://www.who.int/publications/i/item/9789240045064 (date of access 07.05.2025)
8. Yoshino H., Kawase Y. *Ind. Eng. Chem. Res*. **2013**, *52*, 17829-17840.
9. Chen A.H., Liang H.X., Chen T.M., et al. *J. Soils Sediments* **2016**, *16*, 1352-1359.

10. Brady A.R., Vega M.A.P., Stiegler A.N., et al. *ACS EST Water* **2023**, 3, 1352-1363.
11. Ki-Myeong Lee, Joohyun Kim, Jee Yeon Kim, et al. *ACS EST Engg.* **2025**, *5*, 1122–1130.
12. Xin Y.K., Jun J.D., Yu Z.L., et al. *Agr. Water Manage*. **2021**, *250*, 106826.
13. Xu Y.H., Ma Y., Cayuela M.L., et al. *Geoderma*. **2020**, *358*, 113984.
14. Abascal E., Gómez-Coma L., Ortiz I., et al. *Sci. Total Environ*. **2022**, *810*, 152233.
15. Hang D., Hao C., Shepsko Ch., et al. *ACS EST Water* **2023**, *3*, 2989-2995.
16. Wei W., Hu X.Y., Yang S., et al. *Food Res. Int.* **2022**, *152*, 110906.
17. Hu X.Y., Wei W., Zhang J.Y., et al. *Food Biosci.* **2024**, *57*, 103612.
18. Hai Y.L., Jia Y.H., Ze H.L., et al. *ACS EST Water* **2024**, *4*, 5543-5554.
19. Hang D., Hao C., SenGupta A.K. *ACS EST Water* **2021**, *1*, 2275-2283.
20. Werth Ch.J., Chen X.Y., Troutman J.P. *ACS EST Engg.* **2021**, *1*, 6-20.
21. Li Z., Zhai M., Wang X., et al. *ACS Appl. Mater. Inter.* **2024**, *16*, 56134-56145.
22. Hong K. L., Ning G. M., Yun C. L., et al. *ACS Appl. Mater. Inter.* **2024**, *16*, 46312-46322.
23. Yuan C.L., Bai Y.S., Yu H.C., et al. *ACS Catal.* **2024**, *14*, 9797-9811.
24. Xiao Y.S., Xin Y.L., Hong H., et al. *Nano Lett*. **2024**, *24*, 14602-14609.
25. Fang Z.L., Di Z., Fang X.S., et al. *ACS Catal*. **2024**, *14*, 9176-9187.
26. Xiang A., Hao R.W., Xia Z., et al. *ACS Appl. Mater. Inter.* **2025**, *17*, 2844-2862.
27. Ying D.S., Peng S., Ji G.W., et al. *J. Colloid Interface Sci*. **2025**, *686*, 711-721.
28. Jiao J., Yuan Q., Tan M. et al. *Nat. Commun*. **2023**, *14*, 6164.
29. Yang G., Pellessier J., Zi C.D., et al. *ACS Sustainable Chem. Eng*. **2023**, *11*, 7231-7243.
30. Sun Y., Li X., Zhang T., et al. *Angew. Chem. Int. Ed*. **2021**, *60*(30), 21575.
31. Ya Z.Z., Rui H.L., Xia F.T., et al. *J. Am. Chem. Soc*. **2023**, *145*, 3647-3655.
32. Yang Y., Hu C., Shan J., et al. *Angew. Chem. Int. Ed*. **2023**, *62*(20), e202300989.
33. Zhao Y., Zhang Sh., Han C.et al. *Chem. Eng. J.* **2023**, *468*, 143517.
34. Fan X., Bo M.L., Bo W.A., et al. *J. Am. Chem. Soc.* **2024**, *146*, 33569-33578.
35. Kumar G., Dey R.S. Inorg. Chem. **2023**, *62*, 13519-13529.
36. Yan J.L., Ya R.L., Jia H.L., et al. *Ind. Eng. Chem. Res*. **2024**, *63*, 20553-20562.
37. Xiao T.C., Rui L.S., Xiao S.Z., et al. *Langmuir* **2022**, *38*, 4948-4957.
38. Wang X., Xu Y.W., Li Y.H., et al. *Food Chem*. **2021**, *357*, 129762.

Received 11.03.2025
Accepted 07.05.2025